RTTOV-6 - SCIENCE AND VALIDATION REPORT

1. INTRODUCTION AND DOCUMENTATION

The purpose of this report is to document the scientific aspects of the latest version of the fast radiative transfer model, referred to hereafter as RTTOV-6, which are different from the previous model RTTOV-5 and present the results of the validation tests which have been carried out on RTTOV-6. Technical documentation about the software can be found in the RTTOV-6 technical report and an installation and users guide for RTTOV-6 is also available. The enhancements to this version, released in March 2000, have been made within the activities of the EUMETSAT NWP-SAF. The RTTOV-6 software is available to users on request from the Met. Office (email:*rwsaunders@meto.gov.uk*) . The RTTOV-6 documentation can be viewed on the NWP-SAF web site at: http://www.met-office.gov.uk/sec5/NWP/NWPSAF/ and may be updated from time to time.

The baseline document for the original version of RTTOV is available from ECWMF as Eyre (1991). This was recently updated for RTTOV-5 (Saunders *et. al.* 1999a) which can be viewed from the website. Also a relevant paper on RTTOV by Saunders *et. al.* (1999b) is available in the open literature. The changes described below only relate to the differences from RTTOV-5 as described in (Saunders *et. al.* 1999a).

2. SCIENTIFIC CHANGES FROM RTTOV-5 TO RTTOV-6

Only scientific changes between RTTOV-5 and RTTOV-6 are listed here. For technical changes to the software, user interface etc. refer to the RTTOV-6 technical report.

2.1 Activation of cloud liquid water concentration profile

RTTOV-5 only had three profile variables that affected the computed transmittances: temperature, water vapour and ozone from 0.1 to 1013 hPa. For RTTOV-6 cloud liquid water concentration has been added as an additional variable which optionally affects only the microwave channel transmittances. The input cloud liquid water concentration is in units of kg/kg and only layers from the surface to 300 hPa are taken into account in the computation. If the value at the top level of 0.1hPa is set to negative the transmittance calculation is not performed regardless of the input profile. The new cloud code does increase the computational cost of running RTTOV-6 so if the cloud calculations are not required the top level should be set to a negative number. The new code assumes small (size parameter < 1) liquid hydrometeors such that the extinction cross section becomes proportional to the radius cubed (Bohren and Huffman 1983). This is true if scattering is negligible which is a reasonable assumption for non-precipitating liquid water clouds at observation frequencies below 200 GHz. It follows that the extinction per unit mass is independent of radius and thus the sensitivity of changes in optical depth to changes in liquid water mass is independent of the drop-size distribution. This important property allows accurate and efficient calculation of the optical depth if the permittivity of the liquid water is known. For warm cloud emission the permittivity model used in the sea surface emissivity model in RTTOV-5 is adequate but for supercooled water this model gives inaccurate results. There is a wide range of different results from different models for supercooled water because there are very few high quality laboratory measurements. The new code uses a modified version of the model of Liebe et al. (1991) which reproduces the results of the current permittivity model in RTTOV-5 for warm water but fits the original model of Liebe for supercooled water. The drops are assumed to be sufficiently small that scattering can be ignored. Thus the code is only suitable for non-precipitating clouds. Ice extinction is assumed to be zero so the input cloud water profile is all assumed to be liquid. The new cloud model is described in more detail by English et al. (1999).

Validation of the computed cloud liquid water transmittances is difficult as the vertical profile of liquid water is not well represented in NWP models and in situ aircraft data do not measure the top of atmosphere radiance at the same time as the profile measurement. Some comparisons with model fields are described below allowing some conclusions to be drawn.

Model generated liquid water profiles have been used with temperature and humidity profiles to calculate AMSU brightness temperatures for comparison with measured brightness temperatures for two separate six hour assimilation periods in mid-October 1999. Unlike clear air brightness temperatures, which usually show broadly the same features as the NWP model, the cloudy radiances can at times show features completely absent or in different positions compared to the model background. Therefore it is not immediately clear whether modelling the cloudy radiances will give a better or worse fit to the observations. In practise it is found that for those identified as clear in the measurements the fit of the calculated brightness temperatures to the observations is degraded. For those where some cloud is identified the fit is unchanged but for those where deep or precipitating cloud is identified the fit is improved. These results imply that the model has erroneous liquid water in areas identified as clear by the observations. However in regions identified as cloudy by the observations using the model liquid water profiles gives a better fit to the observations than ignoring liquid water effects which is encouraging.

2.2 Addition of default infrared surface emissivity model

RTTOV-5 included an optional model to compute sea surface emissivity for microwave channels called FASTEM described by English and Hewison, (1998). There have been no scientific changes to the FASTEM model in RTTOV-6, although it has been re-coded. For RTTOV-6 an infrared surface emissivity model, ISEM-6, for the sea surface and providing more realistic constant values specified for land has been added. In both cases the models are only invoked if the input surface emissivity is set to zero in which case the output emissivities are those computed by the model.

A full description of the ISEM-6 model and its validation is available in Sherlock (1999). In RTTOV-5 the default emissivity was set to 1. ISEM-6 uses the sea surface values from Masuda *et. al.* (1988) and parameterises them as a function of wavelength and local zenith angle. All wavelengths are covered explicitly with the exception of the VTPR water vapour channel at 19 microns which had to be extrapolated from the Masuda *et. al.* (1988) values. The wind speed dependence is not included with the values at 0 $m.s^{-1}$ taken as representative of all wind speeds. Typical emissivity values of 0.99 to 0.96 are computed for HIRS channel-8 from nadir to 60 deg local zenith angle. The shortwave HIRS channels have lower nadir emissivities (e.g. 0.98 for HIRS-13 and 0.975 for HIRS-19). Over land the value of 1 is replaced by 0.98 and over snow/sea-ice by 0.99 for all infrared channels. It is intended to improve the emissivity computation over land for both infrared and microwave channels in future versions of RTTOV.

2.3 Change to computation of water vapour transmittance for AMSU-B channels

The computation of the water vapour transmittance has always been a weakness of the fixed pressure layer scheme in RTTOV. For RTTOV-6 the water vapour predictors have been changed for the AMSU-B 183.31GHz channels providing a much improved accuracy, compared to RTTOV-5, in the computed transmittances for these channels as shown below in the validation results. The water vapour predictors from DeBlonde (1999) were used. They did not however improve the performance in the infrared water vapour channels and all window channels and so their predictors remain the same as documented in Saunders *et. al.* (1999a).

The simulation of transmittances in RTTOV is based on a regression scheme with a variety of predictors from the profile variables (currently 9) which are related to the layer optical depth, ($d_{i,j}$ - $d_{i,j-1}$), where $d_{i,j}$ is the level to space optical depth for level j and channel i. The regression is actually performed in terms of its departure from a reference profile, for mixed gases, water vapour or ozone:

$$d_{i,j} = d_{i,j-1} + Y_j \sum_{k=1}^{K} a_{i,j,k} X_{k,j} + (d_{i,j}^{ref} - d_{i,j-1}^{ref}) \qquad (1)$$

where K is the number of predictors and their definition (i.e. $X_{k,j}$ and Y_j) are given in Tables 1 and 2, after removing a common factor, Y_j, to simplify the regression. The new predictors are given in the right hand column of Table 1. A more detailed interpretation of the underlying physical processes which govern the choice of predictors is presented in Annex A.

2.4 Changes to dependent sets of line-by-line transmittances

An error in the infrared line-by-line (LbL) GENLN2 transmittances, for the mixed gas reference profile, was corrected which has removed spikes in water vapour Jacobians at the upper levels and slightly improved the computation of infrared stratospheric channel radiances. Transmittance coefficients for all infrared channels were recomputed to remove this error.

The microwave LbL model (Liebe MPM) transmittances have been recomputed on a finer spectral grid to better represent areas of the spectrum where the absorption is varying rapidly with frequency. This has improved the accuracy in the computation of some of the AMSU-A upper and mid-level sounding channel transmittances.

No changes were made to the underlying physics or spectral line databases of either infrared or microwave LbL model for RTTOV-6.

2.5 New instruments supported

RTTOV-5 only supported (A)TOVS, VTPR, and METEOSAT channels. For RTTOV-6 this has been extended to include coefficients for SEVIRI, SSM/I, TRMM/TMI, AVHRR and the GOES imager. A complete list of instruments supported and the actual and *rttov* satellite ids are given in the annex of the RTTOV-6 technical report.

2.6 Revision of profile limits

The profile limits, against which the input profile is checked, as specified in the RTTOV-5 coefficient files were rather conservative and often led to the RTTOV error flag to be returned as non-zero. It was found by experiment that the limits could be widened and the regressions still worked well. These wider limits are now included in the RTTOV-6 coefficient files which will reduce the number of error flags returned. In both versions of the model the transmittance calculation is performed irrespective of whether the input profile is inside or outside the limits specified.

3. VALIDATION OF RTTOV-6

To ensure no bugs have entered in the code during the introduction of the above changes an extensive set of tests were applied to the new model before it was released. These are described below together with the results of the tests. Not all aspects of the model validation are described here, the infrared surface emissivity model validation is described in Sherlock (1999) and the microwave surface emissivity model, FASTEM, in English and Hewison (1998) and the cloud liquid water model in English *et. al.* (1999). The model is validated in several ways:

- The RTTOV-5 and RTTOV-6 transmittances are compared with the LbL model transmittances for the dependent 43 profile TIGR-2 dataset and the 117 ECMWF profile independent set (Chevallier, 1999).

- The RTTOV-5/6 radiances are compared with the radiances computed in the same way as in RTTOV but using the LbL model transmittances for the dependent 43 profile set and the 117 ECMWF profile independent set.

- The RTTOV-5 and RTTOV-6 AMSU radiances have been compared with an independent microwave LbL model ATM and are reported separately by Brunel (2000).

- THE RTTOV-5 and RTTOV-6 radiances and Jacobians have been submitted to the comparison of LbL and fast models for ATOVS channels organised by Garand (1999). This allows a completely independent comparison with several different models.

- There is also an extensive series of comparisons, not described here, between RTTOV-5 and RTTOV-6 transmittances, radiances and jacobians from the TL, AD and K codes to check there are no differences except those anticipated.

The validation results described below are mainly for ATOVS but the performance of the model for new instruments is documented in terms of transmittance differences from the LbL model.

3.1 Validation of transmittances

3.1.1 ATOVS

Some changes are observed when comparing the transmittance predictions of RTTOV-5 and RTTOV-6 for HIRS channels 1 to 4, and the standard deviations of the differences from LbL for the two models are shown in Fig.1. These changes are small in radiance space when compared to the instrument noise, and so they have not been investigated further. However, it is likely that they are due to the change in the GENLN2 transmittances described in sec. 2.4. All other HIRS channels gave the same transmittances for both models.

The use of greater spectral resolution in computing the LbL transmittances for AMSU has brought improvements in RTTOV-6 statistics against LbL even for channels that have retained the RTTOV-5 prediction scheme, as can be seen for the independent set of profiles in Figs. 2 to 4. The AMSU temperature sounding channels 5 to 8 have weighting functions at increasing altitudes through the troposphere because they extend increasingly into the intense complex of close oxygen lines around 60 GHz. While channel 5 samples a single line peak in this band, channels 6,7, and 8 lie in successive troughs; in all cases, greater resolution has brought greater accuracy to the LbL channel-average transmittance, and this has assisted RTTOV-6 in its prediction. Against LbL, neither the bias nor the standard deviation for RTTOV-5 is large enough to warrant concern, but RTTOV-6 has halved the bias at the peak, which represents a path from about 100 hPa to space. As shown in Fig.2 as a percentage of unit transmittance, the greatest improvement in the standard deviation also occurs aloft, and the marked double peak in the standard deviation for RTTOV-5, especially for AMSU 8, has been removed. Longer paths to space involve increased pressure broadening, which is likely to remove any advantage from higher resolution. Although the maximum difference against LbL in channel 5 has become slightly worse nearer the surface, this still represents an improvement over RTTOV-5 in terms of predicted top-of-atmosphere radiance.

AMSU channel 9 lies in the trough between two of the oxygen lines. However, the sidebands of channels 10 to 14 sample closer and closer to the two adjacent line peaks, so their weighting functions are pushed successively higher into the stratosphere where the lines are sharper. Therefore, some similarity to the sequence of results for channels 5 to 8 can be expected, but shifted to higher altitudes. It is interesting that the RTTOV-5 bias for channel 10 differs in sign from all the others (and through to 13 and 14), probably reflecting a change of detail in the simulated intensity distribution across the lines as greater resolution is used. The standard deviations from LbL for channels 9 to 12 are displayed in Fig.3. RTTOV-6 shows a small reduction for channels 10 to 12, but a larger one for channel 9, and the removal, as for channel 8, of the double peaked structure seen for RTTOV-5. In both RTTOV-5 and RTTOV-6, the standard deviations in these channels increase as the weighting functions rise through the stratosphere.

For channels 18-20, RTTOV-6 uses a different scheme for predicting the water vapour transmittance, and this has led to great improvement. The twin sidebands of each of these channels are symmetrically placed about a single absorption feature, the strong line at 183 GHz, with channel 18 nearer the centre, and channels 19 and 20 successively further out, and therefore having weighting functions that peak at lower levels. The reason for this improvement has been discussed in section 2.3. It was found that the new scheme could not be extended to other channels however without a degradation in performance. For channels 18 to 20 the improvement is significant. Indeed the bias peak with respect to LbL in this channel, which is 1% of unit transmittance for RTTOV-5, has been reduced for RTTOV-6 to 0.05%. The corresponding bias improvements for channels 19 and 20, which are more influenced by the surface, are from 0.5% and 0.2% respectively to less than 0.1% in both cases. As can be seen in Fig.4, the effect on the standard deviation is quite dramatic in all three channels, though again less so in channel 20.

3.1.2 SSM/I and TRMM TMI

SSM/I is an instrument newly supported by RTTOV-6, which is why no comparison with RTTOV-5 has been offered. However, the statistics of RTTOV-6 performance in transmittance which are shown in Fig. 5 for the dependent set of profiles. Three of the SSM/I channels are window channels. Those at 19 GHz and 37 GHz lie on either side of the weak water vapour line at 22 GHz, while that at 85GHz lies in a deep trough between the oxygen lines. In clear air conditions the accuracy of RTTOV calculations will depend on the sensitivity of the prediction

scheme to the humidity profile near the surface and also, but more so with increasing frequency, to the contribution of the water vapour continuum along the path to space. As expected, therefore, the standard deviation of the difference from LbL decreases as shorter paths to space are considered. However, even for surface to space, Fig.5 shows very small standard deviations for the two lower frequency windows, with only 0.05% of unit transmittance. Somewhat larger, but still causing no real concern, is the figure of nearly 0.15% at 85 GHz. The remaining channel lies on the 22 GHz water vapour line itself and it was these calculations that dictated the move to higher LbL spectral resolution across the microwave region. This has allowed RTTOV to achieve a satisfactory standard deviation of less than 0.13% of unit transmittance when the entire path is considered from surface to space.

Results for the TMI radiometer on TRMM, which is similar to SSM/I except for the additional window channel at 10.6GHz, have also been computed. Fig. 6 shows very similar standard deviations over the dependent profiles for the channels that correspond closely to SSM/I, and a smaller value, by an order of magnitude, for the window channel at 10.6 GHz. Note the 22 GHz channel covers a slightly different frequency range for both instruments and this is reflected in the differences in the standard deviation of the predicted transmittances plotted in Figs 5 and 6.

3.1.3 SEVIRI, GOES Imager and AVHRR

In the infrared several new instruments are supported by RTTOV-6, but the much greater complexity of the underlying spectrum inevitably leads to similar transmittance differences from LbL as seen with HIRS.

The results for SEVIRI, for the dependent set of profiles, is shown in Fig.7. Note there is no ozone representation in these profiles, which is likely to affect considerably the characteristics of the channel at 9.7μm. The expected increase of standard deviation away from LbL with longer paths to space is evident, reaching around 0.5% of unit transmittance at the surface. Similar results have been obtained for the more opaque channels at 12.0μm and 13.4μm, but for the channel at 3.9μm in the other window the standard deviation is less than half this figure at the surface.

Much greater departures from LbL occur in the humidity channels at 6.2μm, in the most intense part of the water vapour vibration band, and at 7.3μm the low frequency wing. For the latter, with a lower weighting function, the transmittance dispersion tends to increase for the longer paths above the boundary layer, exceeding 1.5% of unit transmittance. At 6.2μm, the dispersion away from LbL peaks in a broad layer between 600 and 100 hPa, where it lies anywhere between 1.5% and 2% of unit transmittance. Figs.8 and 9 show a similar pattern of standard deviations for corresponding channels on the GOES-imager and AVHRR respectively, which are also instruments newly supported by the model. It should be noted that for AVHRR the 3.7μm channel is not predicted as accurately as for SEVIRI and GOES. For the latter this is probably due to the fact that the AVHRR channel is wider taking in more variable gaseous absorption at the shorter wavelengths. The SEVIRI channel is much wider than either however but here the channel response includes the strong CO_2 absorption band which dominates the channel mean transmittance.

2.2 Validation of top of atmosphere radiance

An overall comparison of RTTOV-5 and RTTOV-6 standard deviation against LbL models and the instrumental noise is provided for NOAA-15 and NOAA-14 by the bar-charts in Figs.10 to 12 respectively. Since the values of the fundamental constants have been updated in RTTOV-6 and changes made to both sets of LbL transmittances, the standard deviations from LbL in the HIRS channels show some differences between the two models, although they are small. Both models inevitably show the largest inaccuracy, comparable to the instrument noise, for HIRS channels 8-12, these being dominated by the spectra of variable gases. For MSU, both models lie well below the noise figure of 0.3 K, and the improvement in standard deviation against LbL in RTTOV-6 is probably due to the greater resolution in the LbL calculations that underlie the fast model coefficients. This has also led to improvement in AMSU for NOAA-15, except for a slight degradation apparent in channels 12 and 13 that is still well within the instrument noise. For AMSU channels 18 to 20, however, the effect of the new water vapour prediction scheme is more significant, reducing the standard deviations against LbL well below the noise. As noted earlier, the impact of the new predictors is greatest for channel 18 and decreases in channels 19 and 20 for which surface effects assume more importance.

The corresponding bias comparison for NOAA-15 is shown in Fig.11, and the reduction with RTTOV-6 is particularly significant for AMSU channel 18. The changes in accuracy for HIRS channels 1 to 4 mentioned earlier can also been seen in a bias shift, although this is very small compared to the instrument noise. Significant bias reductions are evident in AMSU channels 5 to 12, but it is interesting that RTTOV-6 reverses and increases the bias for channel 13, while showing little change at all for channel 14.

Finally, a comparison of the NOAA-15 statistics for the dependent 43 profile set and independent 117 ECMWF set is shown in Fig.13, although HIRS channels 1 to 9, which are affected by ozone have been omitted as ozone variability is not included in the dependent profile set. Most channels, except HIRS 13 to 16, show less accuracy for the independent set. As the dependent set has been chosen partly for its diversity, the exceptions are no cause for concern because they involve only small differences. In strict terms, the validation of RTTOV-6 should be based on an independent set and the results for HIRS channel 12 reveals a significant decrease in predictive skill when this is done. This justifies the large additional burden of LbL computation this involves for the independent set.

2.3 Validation of Jacobians

The jacobians for RTTOV-5 and RTTOV-6 were compared for all ATOVS and TOVS channels and found to be very similar, with the exception of AMSU channels 18-20. A few of the spikes in the upper layers of all the water vapour jacobians of RTTOV-5 have been removed in the RTTOV-6 model.

The jacobians for a selection of HIRS and AMSU channels for both RTTOV-5 and RTTOV-6 have been submitted to the Garand intercomparison, which includes LbL model jacobians to compare with. This provides an independent validation of the RTTOV-6 jacobians (and also transmittances and radiances). The full set of validation results can be viewed at http://www.cmc.ec.gc.ca/rpn/arma/intercomparison/ which provides links to both tables and plots some of which are reproduced below. For HIRS channels 2, 5, 9, 10, 11, 12 and AMSU channels 6, 10, 14 and 18 jacobians for 5 diverse profiles are computed. Temperature, water vapour and (for HIRS only) ozone jacobians have all been computed and Garand presents tables of the "goodness of fit" of the fast models to an assigned LbL model. This "goodness of fit" should be treated with caution as spikes in the top level can dominate the value when in fact the general shape of the jacobian can be good. Nevertheless they are a useful way to summarise the results and Figure 14 has been prepared comparing RTTOV-5 and 6, SYNSATRAD (IR only) and OPTRAN. For the HIRS channels the fit to the GENLN2 jacobians is used as they are the reference for RTTOV and OPTRAN. SYNSATRAD is included as a semi-fast model but based on a different LbL model. For the AMSU channels AESMWLBL (which is based on Liebe MPM-89/92) is used as the reference for RTTOV and the microwave model labelled LBLRTM is used as the reference for OPTRAN. Garand's qualitative guidance is that "goodness of fit" values of less than 10 is good, 10-20 fair and >20 bad.

For the temperature jacobians (top panel of Fig. 14) in general the RTTOV computations are close to the LbL model, with a few exceptions, and have similar or better fits than OPTRAN (except HIRS-12). SYNSATRAD has better fits to GENLN2 in all channels (except HIRS-5) in spite of not being based on GENLN2. HIRS channels 10, 11 and 12 show some divergence from the LbL model jacobians around the peaks. For instance Figure 15 shows the temperature jacobians for HIRS channel 11 and between 600-700hPa both RTTOV models diverge from the other models especially for profile 19. This is almost certainly related to the water vapour predictors of RTTOV. There is also a spike in the jacobian at 100hPa for HIRS channel 9, profile 18 (and to a lesser extent other profiles) which is at variance with all the other models (see plot on web site above) which explains the higher value for this channel. The AMSU channels are in good agreement, with one exception, AMSU channel 14 (38). RTTOV agrees with the LbL model on which it was based (hence the small values in Fig. 14) but this LbL model differs significantly from others for this channel so the LbL model may be in error as some of the other models do give a more realistic shape to the jacobian above 2hPa.

For the water vapour jacobians (bottom panel of Fig. 14) HIRS channels 10, 11 and 12 all have poor fits to the LbL models relative to OPTRAN and SYNSATRAD. This is also illustrated in Figure 16 for HIRS channel 10 (the worst case). This underlines the need to improve the prediction for these infrared water vapour channels. All models have poor fits for HIRS channels 5 and 9 but these have a lower sensitivity to water vapour. For the AMSU water vapour channel 18 (38) a definite improvement for RTTOV-6 jacobians is seen over RTTOV-5 when compared with AESMWLBL.

For all the HIRS channel ozone jacobians the agreement of RTTOV with the LbL models is reasonable throughout (much better than OPTRAN) although SYNSATRAD is significantly better (e.g. for HIRS channel 9 see lower panel of Fig 14).

2.4 Comparison of RTTOV-6 with RTSSMI

A fast RT model based on RTTOV, but with a different sea surface emissivity model, was developed by Phalippou (1996) and has been used in an operational 1DVar retrieval at ECMWF and the Met. Office for several years. Hereafter this model is referred to as RTSSMI. It is planned at both centres to replace this model with the generic RTTOV code to unify all the RT models in the assimilation code now that cloud liquid water is activated for the microwave channels. Before doing this it is important to compare both models in terms of atmospheric transmittance, surface emissivity and sensitivity of surface emissivity to wind speed to the microwave surface emissivity model. Note that this comparison will also be relevant for other microwave radiometer simulated radiances (e.g. AMSU, TMI). The comparisons below are all done for the SSM/I zenith angle of 53.1 deg and the channels 19.35GHz (V) and (H), 22.235GHz (V), 37GHz (V) and (H), 85.5GHz (V) and (H) referred to as channels 1-7 respectively below.

A set of 26 diverse atmospheric profiles over the ocean was used to investigate the differences between RTSSMI and RTTOV-6. Figure 17 shows the mean RT model difference for the SSM/I channels for 3 different wind speed regimes together with the mean global observed-NWP model first guess values for DMSP F-13 SSM/I (for the Met. Office NWP model simulated using RTSSMI). Differences between the RT models are between –2K and +5.5K but it is encouraging for RTTOV-6 that the differences are in the same sense as the NWP model biases. The model radiance differences are mainly due to the different surface emissivities computed by the models which have emissivity differences of up to 0.05 at 10m.s^{-1} wind speeds. However these emissivities are not strictly comparable as for RTTOV-6 the FASTEM values include a correction for non-specular reflection. The transmittance profiles are very similar for both models for all profiles.

An important quantity for retrieval/radiance assimilation is the sensitivity of the radiances (T_B) to surface wind speed (w_s) as this governs how the measured radiances can influence the model wind speed. Figure 18 compares the sensitivities (dT_B/dw_s) for each channel at 0, 3 and 10m.s^{-1} and for 2 different SST regimes below and above 290K. Figure 18 shows the H-polarisation channels are much more sensitive to windspeed than the V-pol channels. The sensitivity of RTSSMI varies more with SST (closer agreement with FASTEM for SSTs >290K, except channel 7) whereas FASTEM is not strongly influenced by SST. The RTSSMI windspeed sensitivity for channel 2 is half that for FASTEM at zero windspeed with both models converging at higher windspeeds and SSTs. For the other channels RTSSMI is generally more sensitive than FASTEM.

There are several possible reasons for the differences seen in the computed sea surface emissivity and sensitivities to wind speed between the two models. For the absolute emissivity values RTSSMI uses the Ulaby et. al. (1986) model whereas FASTEM uses the more modern PIOM permittivity model (Lamkaouchi et. al. 1997). It is believed the PIOM model is more accurate. For the sensitivity to surface windspeed the surface roughness, foam model and treatment of non-specular reflection can cause differences. The surface roughness model is similar enough for SSM/I channels to not explain the differences computed. The FOAM model is different in FASTEM (Monahon and O'Muircheartaigh, 1986) to RTSSMI (Monahon and O'Muircheartaigh, 1980). It is hard to decide which model is more realistic (a small sample of aircraft data suggest the former is better). The differences only become significant above 12m.s^{-1} (~0.75% at 12m.s^{-1}, 2% at 15m.s^{-1}) so are relatively rare. Finally the treatment of the non-specular reflected radiance is different between the two models. FASTEM makes no allowance for the sensitivity of the non-specular correction to variations in the atmospheric downwelling radiation whereas RTSSMI models this effect (which is why it is much slower). This results in too high sensitivities for FASTEM at low windspeeds and large zenith angles, but the error reduces in the tropics and for the more opaque channels (i.e. channels 6/7) where the downwelling radiation is higher. This may explain the differences between the two models at low windspeeds shown in Figure 18. Note this is not considered a problem for AMSU except at the fields of view at the edges of the swath.

In summary the treatment of non-specular reflection in RTSSMI may still be superior to FASTEM. The treatment

of foam and permittivity model is believed to be better in FASTEM. The atmospheric transmittances are very similar for both models. It is planned both at ECMWF and The Met. Office to experiment with RTTOV-6 in NWP assimilation mode within the coming months to investigate the differences further. An improved treatment of non-specular reflection in RTTOV is also being investigated.

3. SUMMARY

The new fast radiative transfer model RTTOV-6 has been shown to be an overall improvement to the previous model RTTOV-5 particularly for the AMSU-B water vapour channels. It now also supports a much greater range of satellite instruments and sea surface emissivity at infrared wavelengths and cloud liquid water transmittance in the microwave can now be modelled.

As part of the NWP-SAF programme more improvements to the model are planned for 2001. In particular the code will be rewritten in FORTRAN-90 and be prepared for including simulations of the high spectral resolution sounders (i.e. AIRS and IASI). Users of the code are invited to submit comments or report bugs to rwsaunders@meto.gov.uk. An RTTOV email newsgroup exists to share experiences.

4. REFERENCES

Bohren, C.F. and D.R. Huffman 1983 Absorption and scattering by small particles *Wiley-Interscience 530pp*.

Brunel, P. 2000 Report on validation of RTTOV-5 AMSU simulated radiances with ATM line-by-line *NWP SAF report*

Chevallier, F. 1999 TIGR-like sampled databases of atmospheric profiles from the ECMWF 50-level forecast model. *NWP-SAF programme research report 1*.

DeBlonde, G. 1999 Variational retrievals of humidity using DMSP SSM/T-2 brightness temperatures. *Proc. ITSC-10 Boulder Colorado, 27 Jan-2 Feb 1999 12pp*

English S.J. and T.J. Hewison 1998 A fast generic millimetre wave emissivity model. *Microwave Remote Sensing of the Atmosphere and Environment Proc. SPIE* **3503** *22-30*

English S.J., C. Poulsen and A.J. Smith 1999 Forward modelling for liquid water cloud and land surface emissivity *Proceedings of ECMWF workshop on ATOVS*, ECMWF, Reading, UK, 2-5 November 1999, *To be published by ECMWF*

Eyre J.R. 1991 A fast radiative transfer model for satellite sounding systems. *ECMWF Research Dept. Tech. Memo.* **176** *(available from the librarian at ECMWF).*

Garand, L. 1999 Results from the HIRS-AMSU intercomparison of radiative transfer codes. *In Proc. of workshop Use of ATOVS Data in NWP Assimilation. Reading, U.K. 2-5 Nov 1999*

Lamkaouchi K., A. Balana and W.J. Ellison 1997: New permittivity data for sea water (30-100 GHz). Extension of ESA report 11197/94/NL/CN.

Liebe H.J., G.A. Hufford, T. Manabe 1991 A model for the complex permittivity of water at frequencies below 1 THz, *Int. J. Infrared and Millimetre Waves* **12** *659-671*.

Masuda, K., T. Takashima and Y. Takayama. 1988 Emissivity of pure and sea waters for the model sea surface in the infrared window regions. *Rem. Sens. Env.* **24** *313-329.*

Monohan, E.C. and I. G. O'Muircheartaigh, 1980 Optimal power law description of oceanic whitecap coverage dependence on windspeed. *J. Phys. Oceanogr.***10,** *2094-2099.*

Monohan, E.C. and I. G. O'Muircheartaigh, 1986 Whitecaps and the passive remote sensing of the ocean surface. Review article. *Int. J. Remote Sens.* **7** *627-642*.

Phalippou, L. 1996 Variational retrieval for humidity profile, wind speed and cloud liquid water path with the SSM/I: Potential for numerical weather prediction. *QJRMS,* **122,** 327-356.

Saunders R.W., M. Matricardi and P. Brunel 1999a A fast radiative transfer model for assimilation of satellite radiance observations - RTTOV-5. *ECMWF Research Dept. Tech. Memo.* **282** *(available from the librarian at ECMWF).*

Saunders R.W., M. Matricardi and P. Brunel 1999b An Improved Fast Radiative Transfer Model for Assimilation of Satellite Radiance Observations. *QJRMS,* **125,** 1407-1425.

Sherlock, V.J. 1999 ISEM-6: Infrared Surface Emissivity Model for RTTOV-6. *NWP Tech. Rep. 287 (available from Met. Office Librarian).*

Ulaby, F.T., R.K. Moore and A.K. Fung 1981 Microwave Remote Sensing vol 3 From theory to applications. *Artech. House Inc.*

Predictor	mixed gases	HIRS water vapour/ ozone	AMSU window water vapour	AMSU-B Water line
X_{1j}	$\delta T_j \sec\theta$	δT_j	δT_j	δT_j
X_{2j}	$\delta T_j^2 \sec\theta$	$\overline{p\,\delta T_j}$	$\overline{p\,\delta T_j}$	$\overline{p\,\delta T_j}$
X_{3j}	$\overline{\delta T_j} \sec\theta$	δq_j	δq_j	δq_j
X_{4j}	$\overline{p\,\delta T_j} \sec\theta$	$\overline{p\,\delta q_j}$	$\overline{p\,\delta q_j}$	$\overline{p\,\delta q_j}$
X_{5j}	$(\sec\theta - 1)$	$\delta T_j (\sec\theta\, u_j)^{1/2}$	$\delta T_j (u_j)^{1/2}$	$\delta T_j (\sec\theta\, u_j)$
X_{6j}	$(\sec\theta - 1)^2$	$\delta T_j^2 (\sec\theta\, u_j)^{1/2}$	$\delta T_j^2 (u_j)^{1/2}$	$\delta T_j^2 (\sec\theta\, u_j)$
X_{7j}	$\overline{\delta T_j}(\sec\theta - 1)$	$\delta q_j (\sec\theta\, u_j)^{1/2}$	$\delta q_j (u_j)^{1/2}$	$\delta q_j (\sec\theta\, u_j)$
X_{8j}	$\overline{p\,\delta T_j}(\sec\theta - 1)$	$(\sec\theta - 1)(\sec\theta\, u_j)^{1/2}$	0	$\delta q_j^2 (\sec\theta\, u_j)$
X_{9j}	$\overline{\delta T_j}(\sec\theta - 1)$	$(\sec\theta - 1)^2 (\sec\theta\, u_j)^{1/2}$	0	$\delta T \delta q_j (\sec\theta\, u_j)$
Y_j	***1***	$(\sec\theta\, u_j)^{1/2}$	$\sec\theta (u_j)^{1/2}$	$(\sec\theta\, u_j)$

Table 1: RTTOV-6 predictors for mixed gases, water vapour and ozone. The profile variables are defined in Table 2 below.

$$\overline{\delta T_j} = \frac{1}{p_j}\sum_{\ell=1}^{j} \delta T_\ell (p_\ell - p_{\ell-1}) \qquad u_j = \tfrac{1}{2}(q_j + q_{j-1})(p_j - p_{j-1})$$

$$\overline{p\,\delta T_j} = \frac{2}{p_j^2}\sum_{\ell=1}^{j} p_\ell \delta T_\ell (p_\ell - p_{\ell-1}) \qquad \overline{p\,\delta q_j} = \frac{2}{p_j^2}\sum_{\ell=1}^{j} p_\ell\, \delta q_\ell (p_\ell - p_{\ell-1})$$

$$\delta T_j = \tfrac{1}{2}\left(T_j - T_j^{ref} + T_{j-1} - T_{j-1}^{ref} \right) \qquad \delta q_j = \tfrac{1}{2}\left(q_j - q_j^{ref} + q_{j-1} - q_{j-1}^{ref}\right)$$

T_j and q_j are the temperature and specific humidity or ozone volume mixing ratio profiles. T_j^{ref} and q_j^{ref} are corresponding reference profiles (the mean of a set of global water vapour and ozone profiles has been used).

Table 2: Definition of profile variables used in predictors defined in Table 1.

Annex-A: Physical basis for RTTOV transmittance predictors

A Line by Line (LbL) calculation of the slant-path optical depth at angle $sec(\theta)$ through the jth layer of an atmospheric profile will be monochromatic in nature, producing the ordinate of a spectral function or density at a specific set of frequencies. In a layer with column density u_j of radiating molecules, the contribution from a single radiating molecule to the optical depth must be scaled by a path factor of $sec(\theta)\, u_j$, since this governs the overall number of contributing absorbers.

RTTOV, on the other hand, calculates the channel i averaged optical depth, and this also depends on the spectral variation within the channel. In the infrared, where this will involve a multitude of spectral lines, the growth in the channel-averaged absorption across the layer still provides a path factor of $sec(\theta)\, u_j$ for weak absorption. However, the variation will be less when the absorption is strong, and a path factor of $(sec(\theta)\, u_j)^{1/2}$ is then likely to be more appropriate (Goody & Yung 1989).

In either case, the width of each contributing line depends on the molecular collision rate, and therefore has a `foreign-collision' part that is fixed, and a 'self-collision' part proportional to u_j . For frequencies sufficiently far from the line centre, the self dependency on u_j is the main factor which provides a simple linear scaling with u_j and the path factor. In a LbL calculation, therefore, the foreign and self contributions to the monochromatic optical depth can be expected to vary respectively as $sec(\theta)\, u_j$ and $sec(\theta)\, u_j^2$ whereas the weak and strong cases distinguished by channel averaging in RTTOV leads to the appearance of more complicated dependencies on the abundance, as shown in Table 1.

The starting point for generating predictors for RTTOV is the multivariate Taylor expansion of the monochromatic expression for the layer optical depth about the values of path variables in the corresponding layer of a reference profile. The predictors are chosen from among the low order departures that appear in this linear combination, and the coefficients have their value determined by regression.

For well-mixed gases, RTTOV is able to treat the absorber abundance as a constant in each layer and the predictors need only take account of departures δT_j, and $sec(\theta\text{-}1)$ from reference in the layer temperature and viewing angle, as shown in the second column of Table 1. Since RTTOV must compute channel-averaged radiation, additional predictors that refer to the overlying layers, those shown with overbars and defined in Table 2, are also included. For variable gases however, predictors based on the departure δq_j in the layer abundance of the absorber will be necessary and the column abundance $sec(\theta)\, u_j$ across the layer will be involved in different ways for weak and strong absorption.

The third column of Table 1 relates only to infrared channels. After taking account of the common factor, Y_j, here $(sec(\theta) u_j)^{1/2}$, predictors X_{1j} to X_{4j} and X_{5j} to X_{9j} relate respectively to the strong and the weak cases. However, the channels in a microwave instrument like AMSU are either in a water vapour window or near the single strong and relatively broad line of water vapour at 183.31 GHz. Unlike an infrared channel, they sample from a relatively slow spectral variation, and therefore present a rather different problem.

The current RTTOV treatment of water vapour for microwave channels is shown in the last two columns of the Table. In RTTOV-5, the predictor set for all AMSU channels is that shown in the fourth column of the Table, and, for channels in the water window, the same is also true of RTTOV-6. For channels near the 183 GHz line, however, RTTOV-6 drops the distinction by strength and includes both linear and quadratic path factors, as shown in the very last column of Table 1. Compared to the scheme retained for the infrared, RTTOV-6 appears to go further than its predecessor in moving the microwave scheme towards the monochromatic variation with abundance used for the LbL calculation, and this may account for some of its success.

Goody R.M and Y.L. Yung 1989, Atmospheric radiation, Oxford (Sec.4.2).

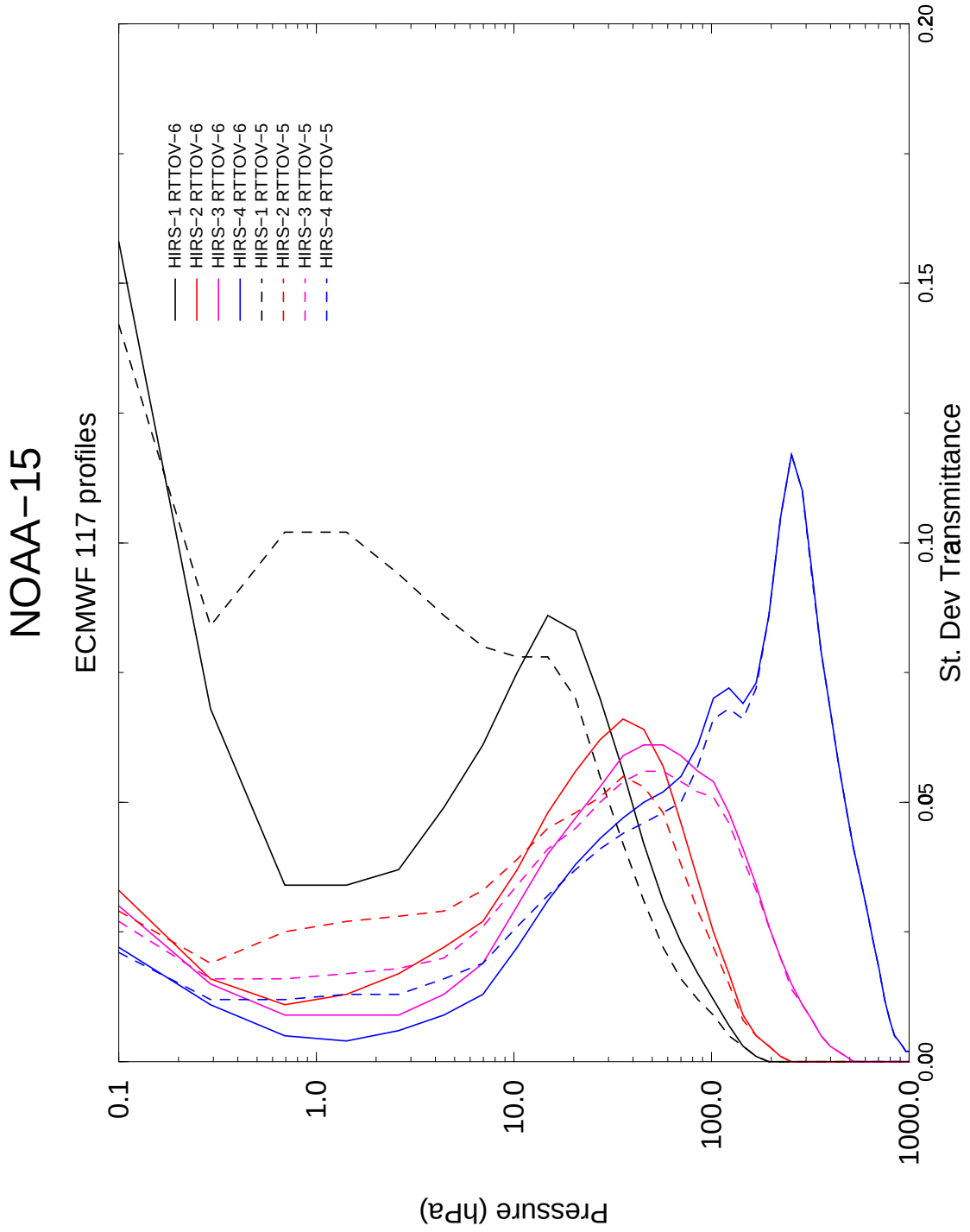

Figure 1 Standard Deviation of RTTOV-5 and RTTOV-6 HIRS transmittance differences from GENLN2 LbL model

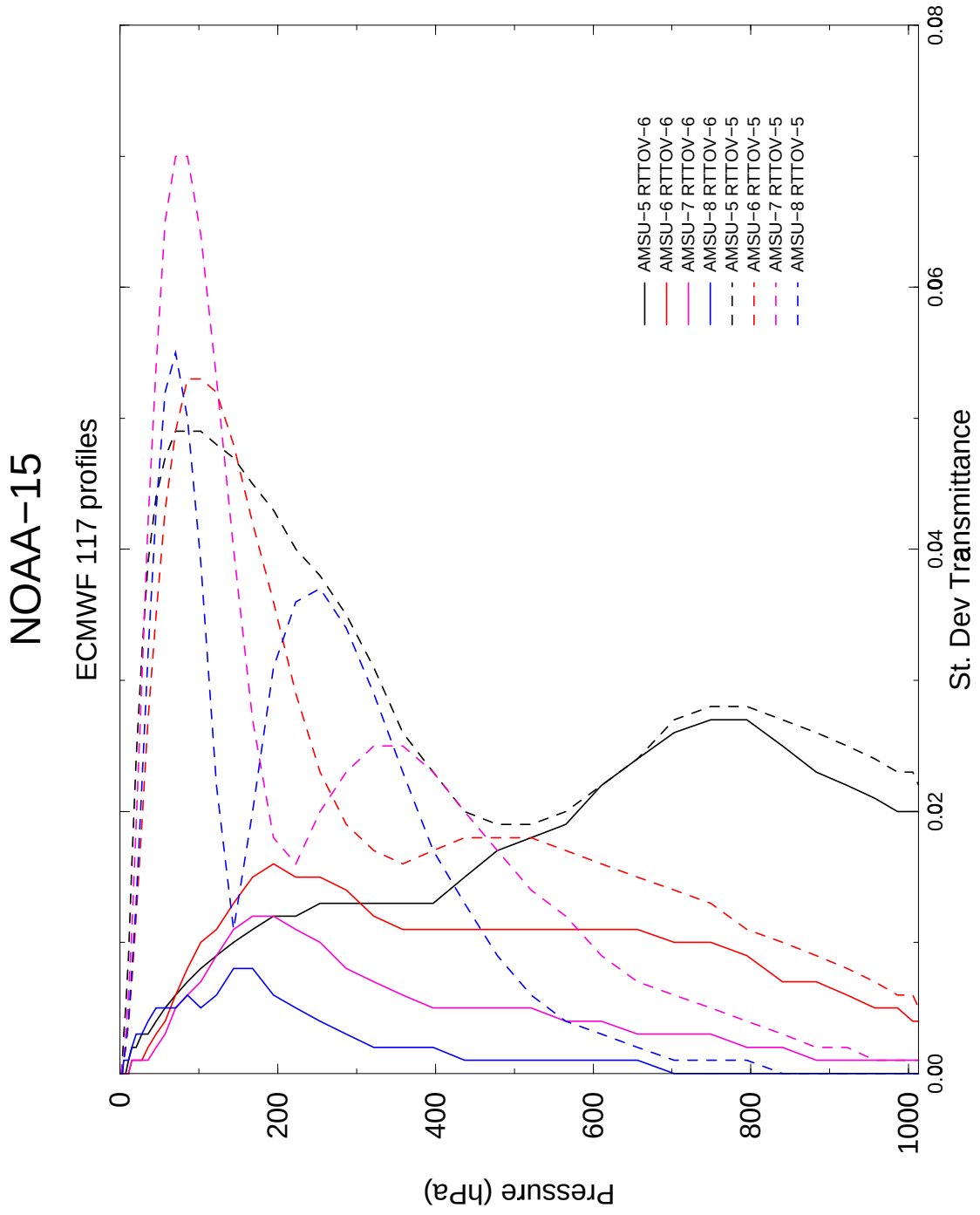

Figure 2 Standard deviation of RTTOV-5 and RTTOV-6 AMSU-A transmittance differences from MPM LbL model

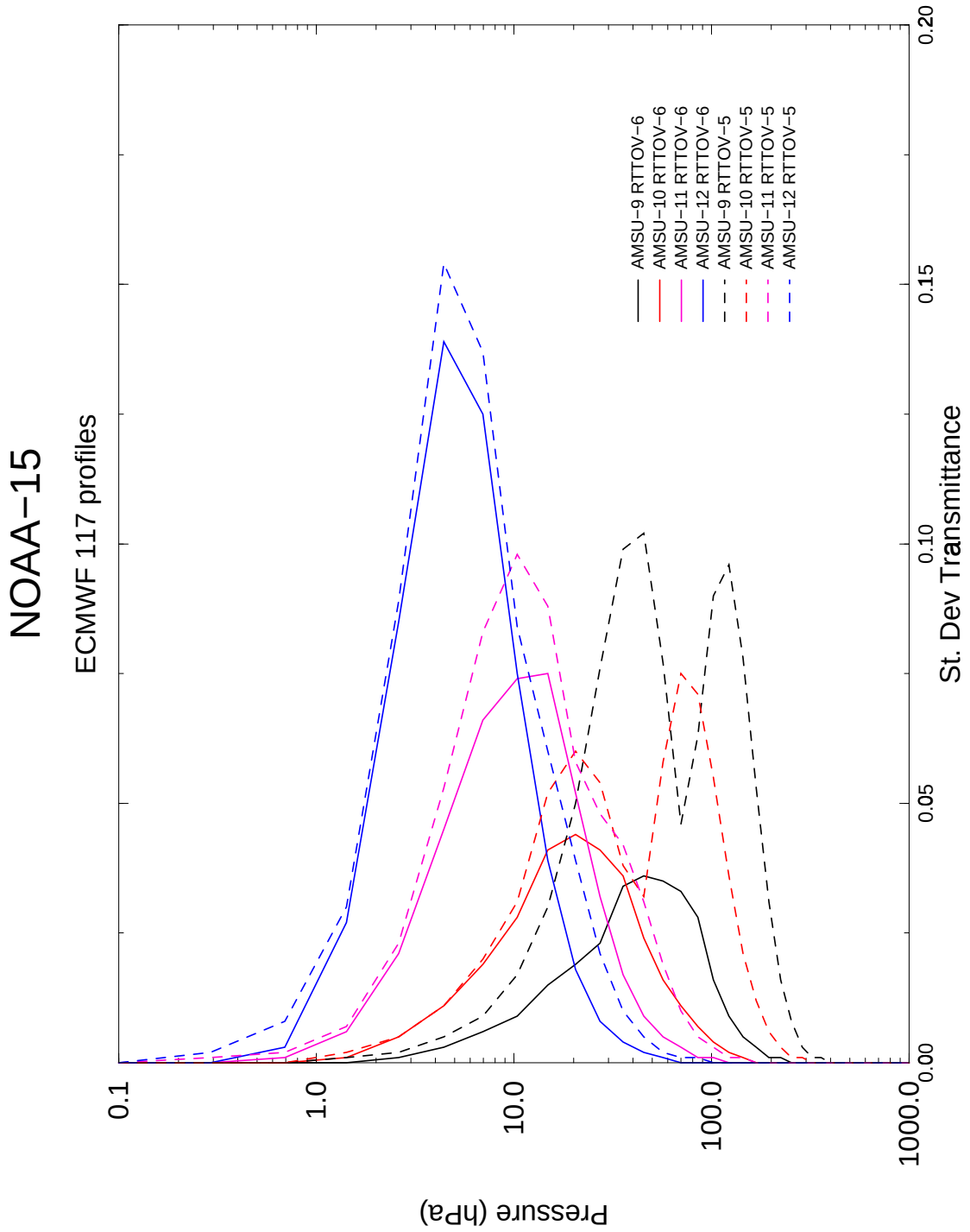

Figure 3 Standard deviation of RTTOV-5 and RTTOV-6 AMSU-A transmittance differences from MPM LbL model

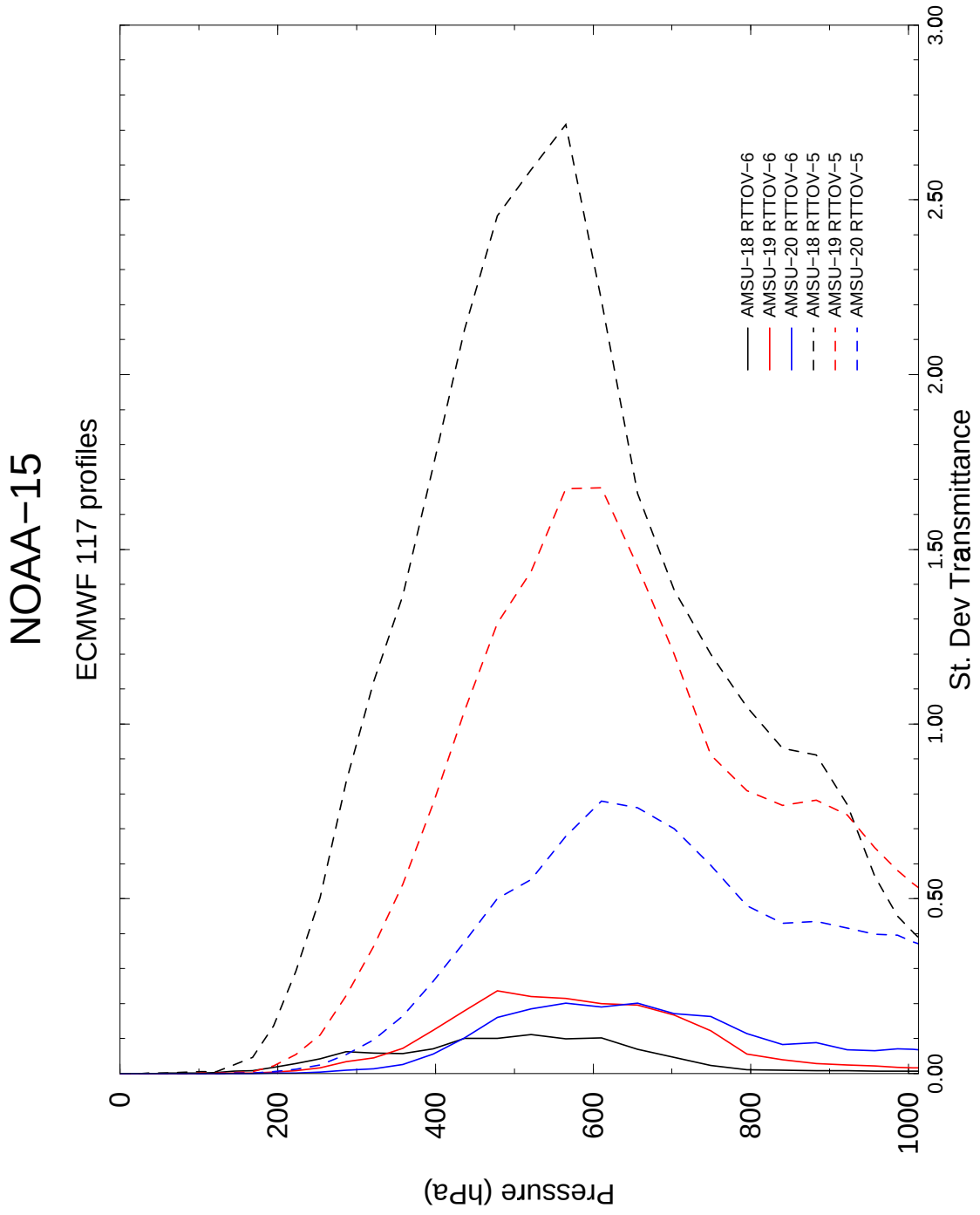

Figure 4 Standard deviation of RTTOV-5 and RTTOV-6 AMSU-B transmittance differences from MPM LbL model

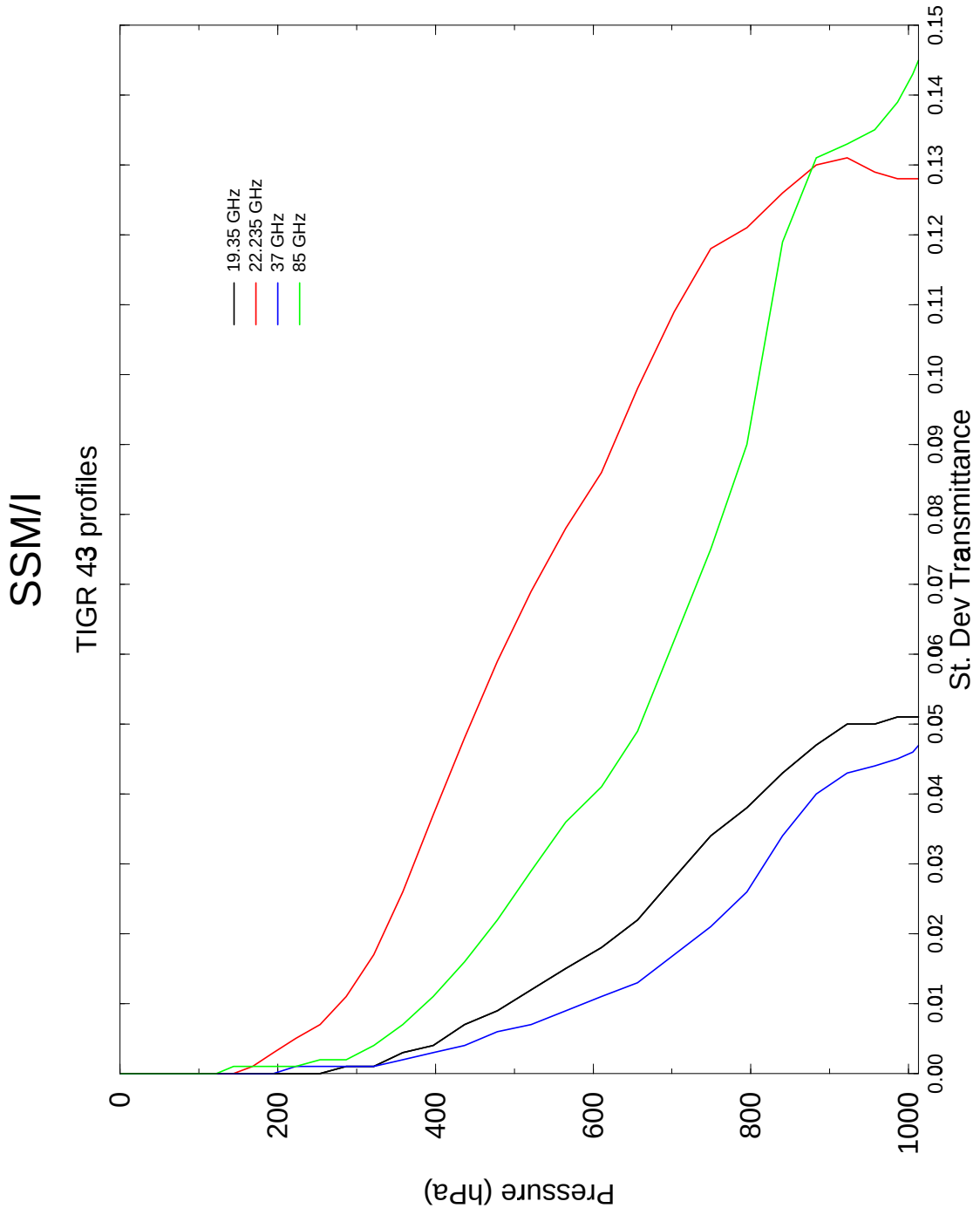

Figure 5 Standard deviation of RTTOV-6 SSM/I transmittance differences from MPM LbL model

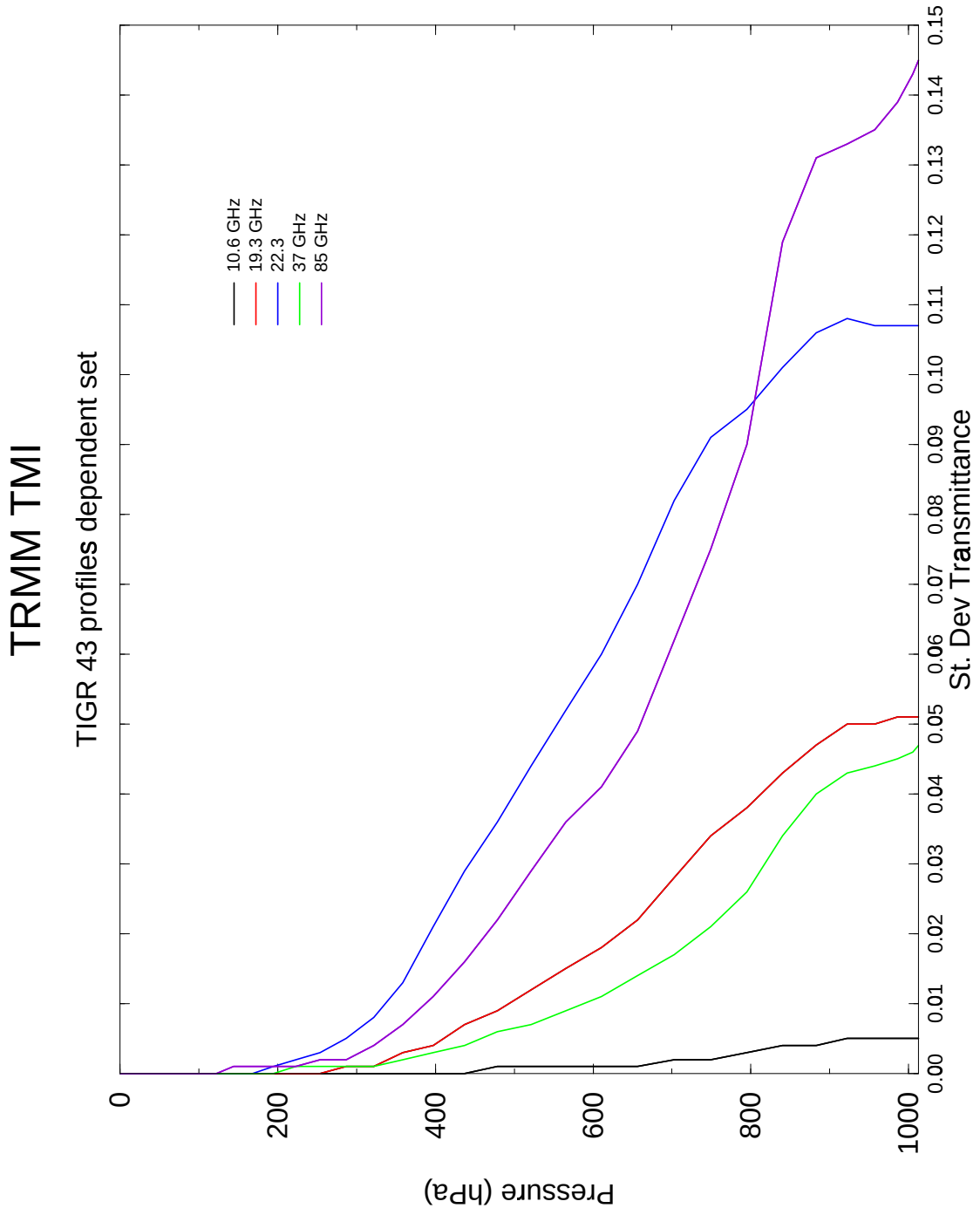

Figure 6 Standard deviation of RTTOV-6 TMI transmittance differences from MPM LbL model

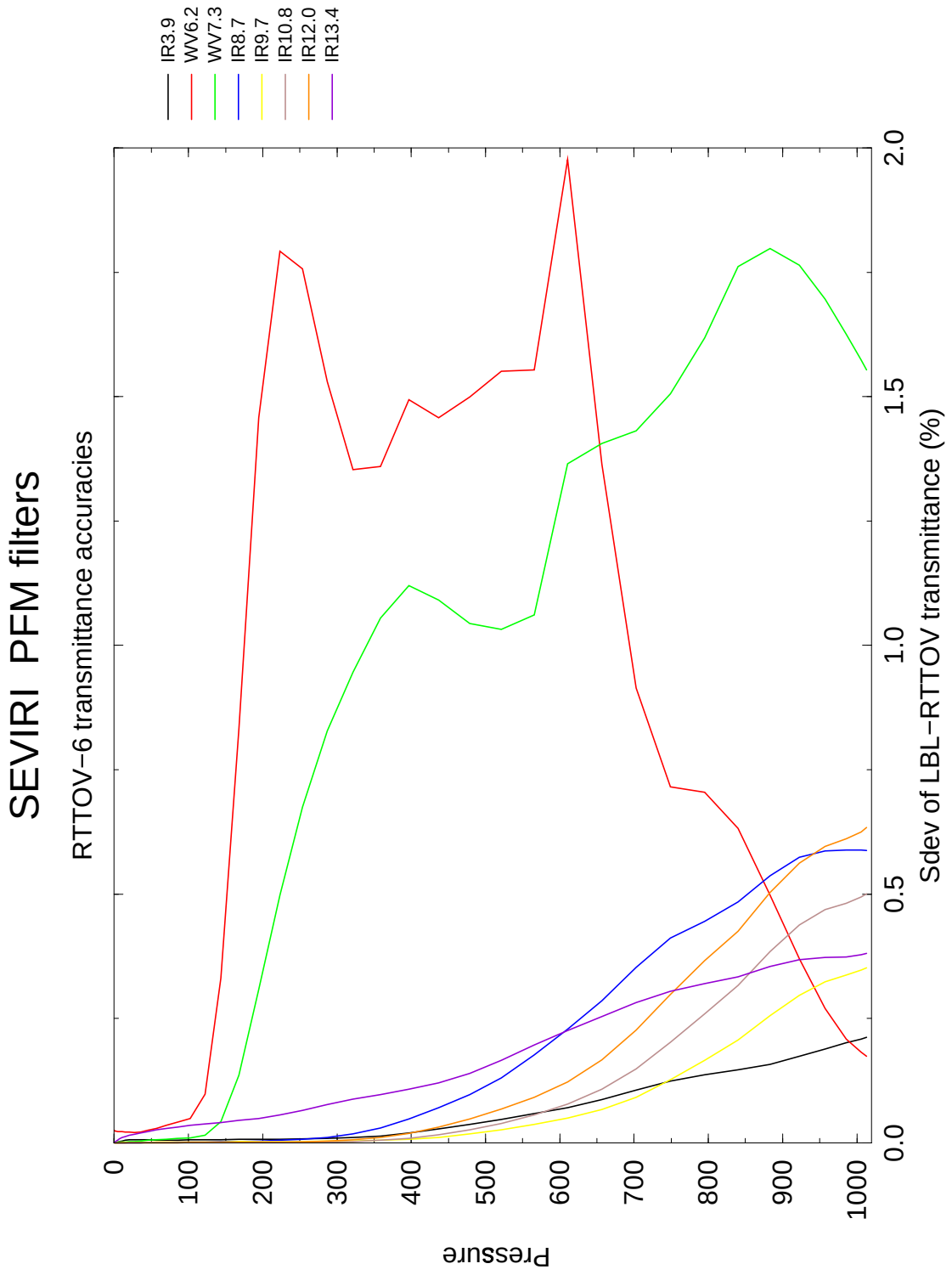

Figure 7 Standard deviation of RTTOV-6 SEVIRI PFM transmittance differences from GENLN2 LbL model for 43 profile dependent set.

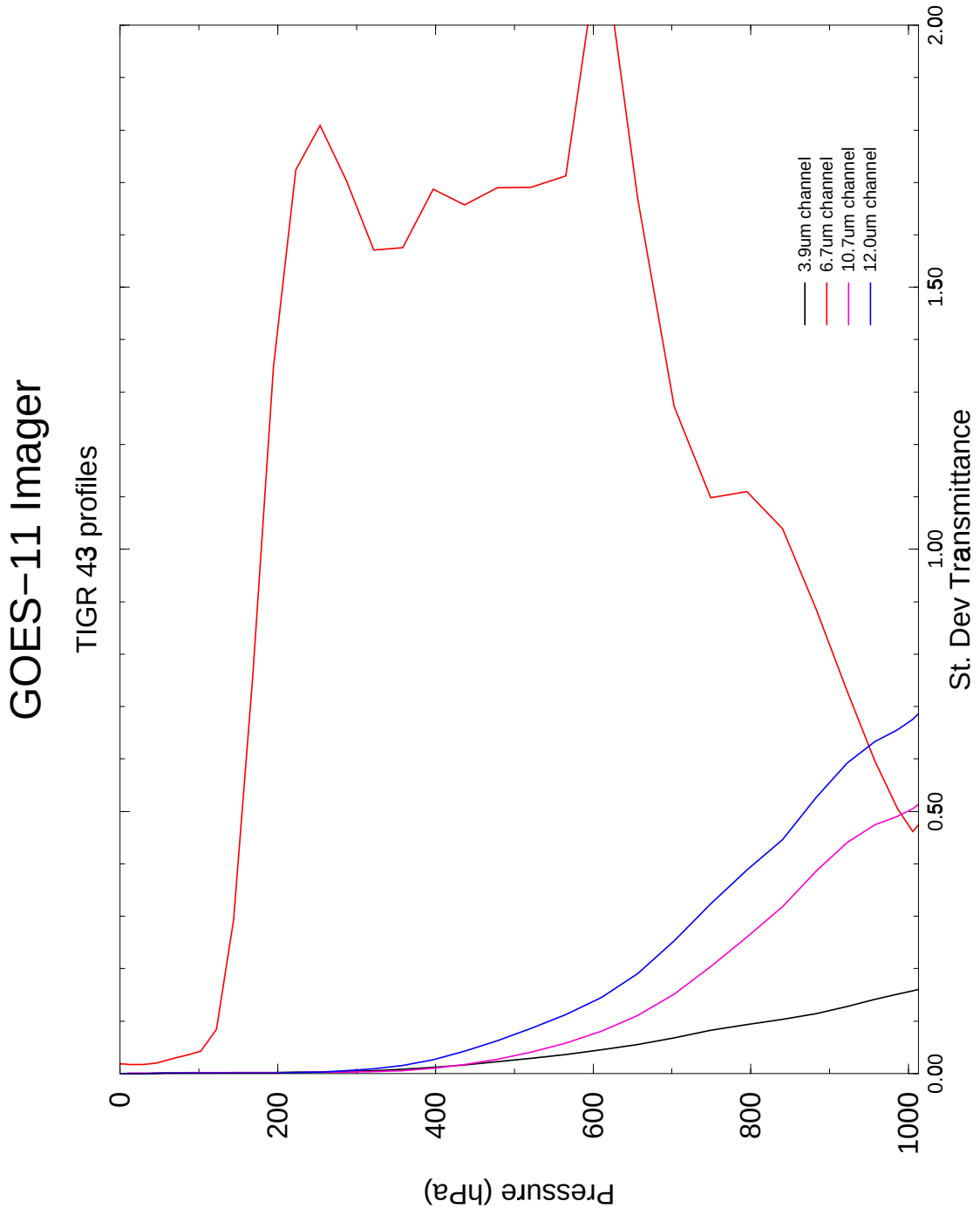

Figure 8 Standard deviation of RTTOV-6 GOES imager transmittance differences from GENLN2 LbL model for 43 profile dependent set.

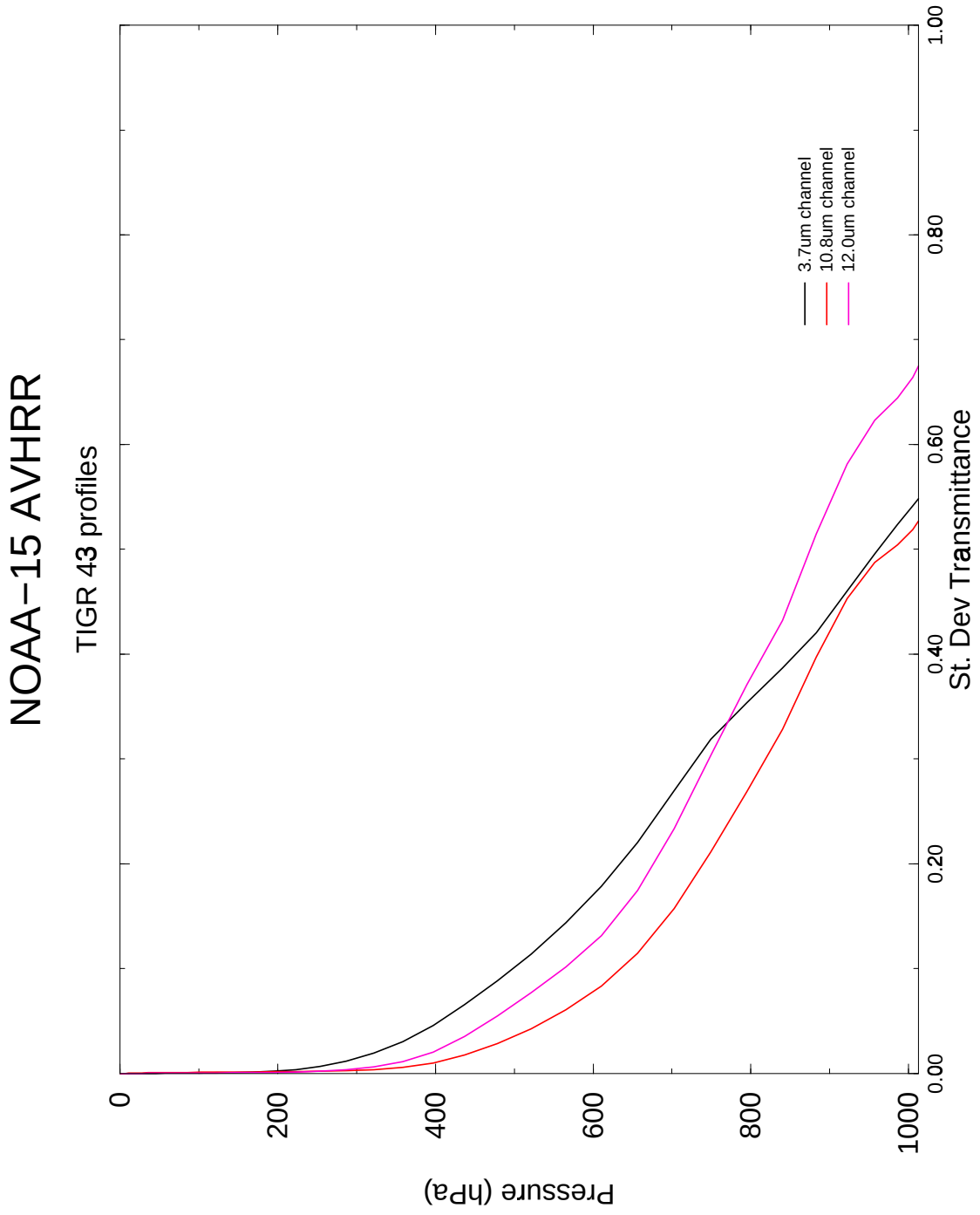

Figure 9 Standard deviation of RTTOV-6 AVHRR transmittance differences from GENLN2 LbL model for 43 profile dependent set.

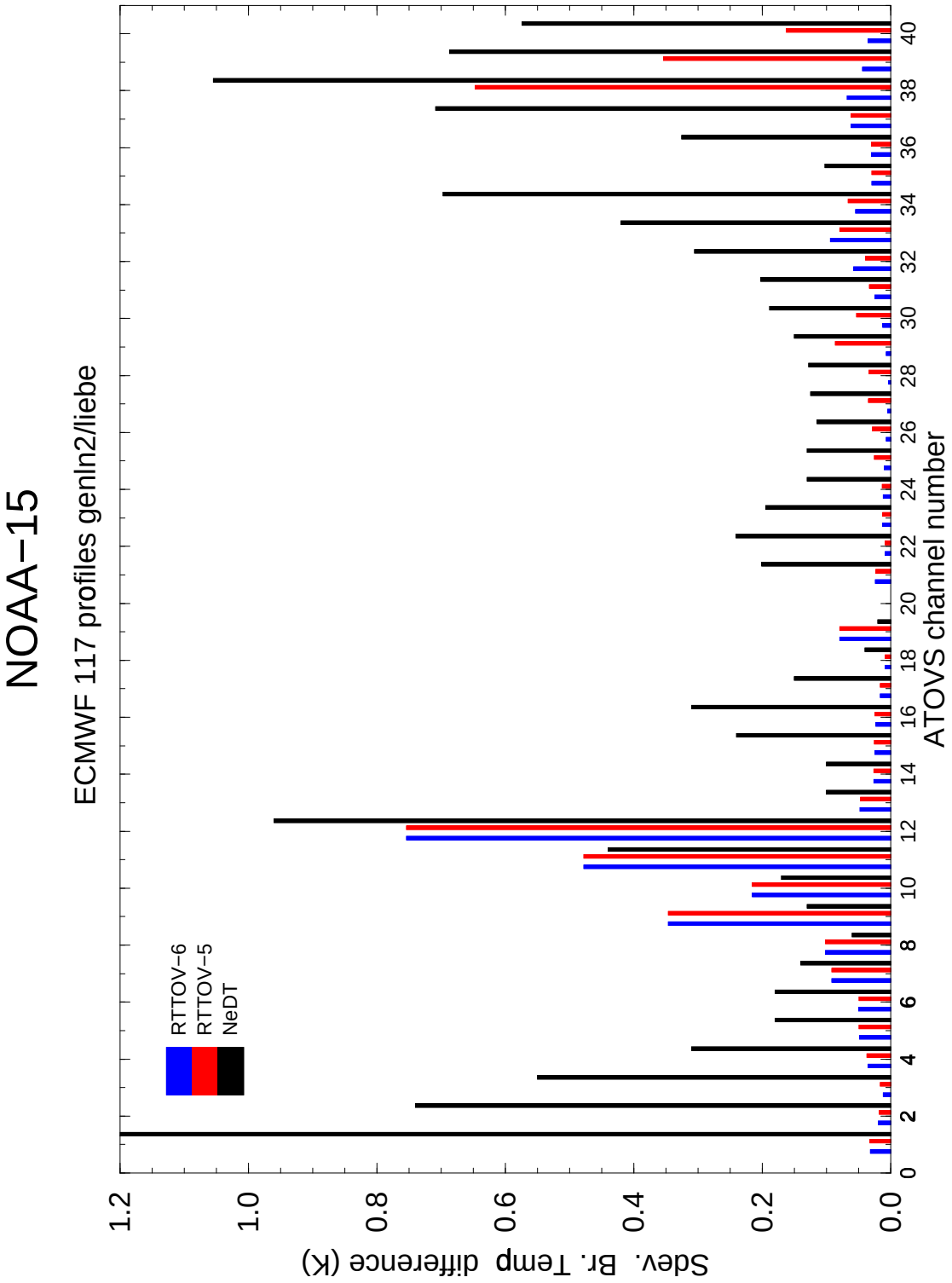

Figure 10 Standard deviations of RTTOV-5 and RTTOV-6 top of atmosphere brightness temperature differences from LbL for the 117 independent profile set for NOAA-15 ATOVS. Channels 1-20 are HIRS, 21-40 AMSU.

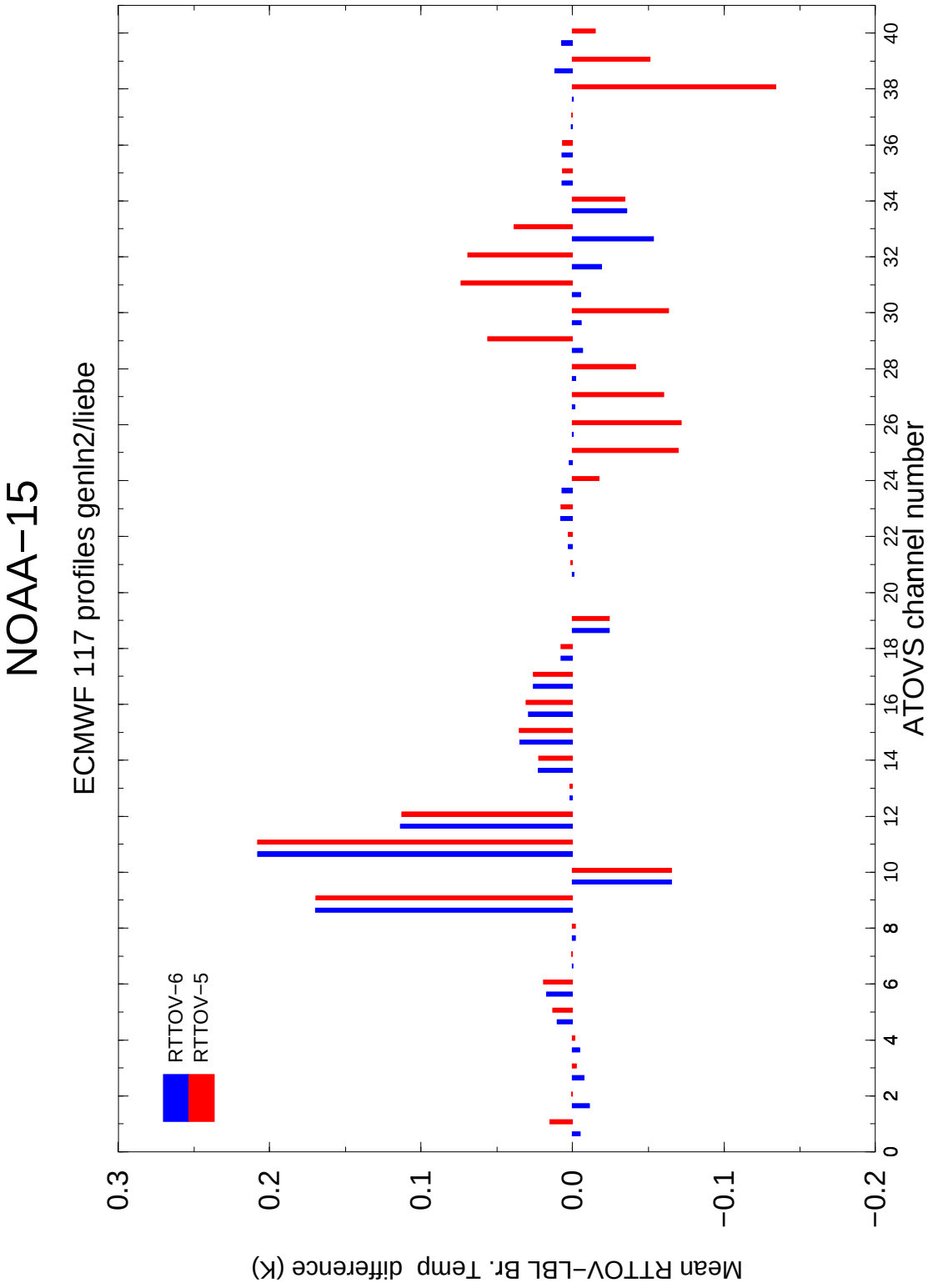

Figure 11 Same as Figure 10 but for the mean difference in brightness temperature.

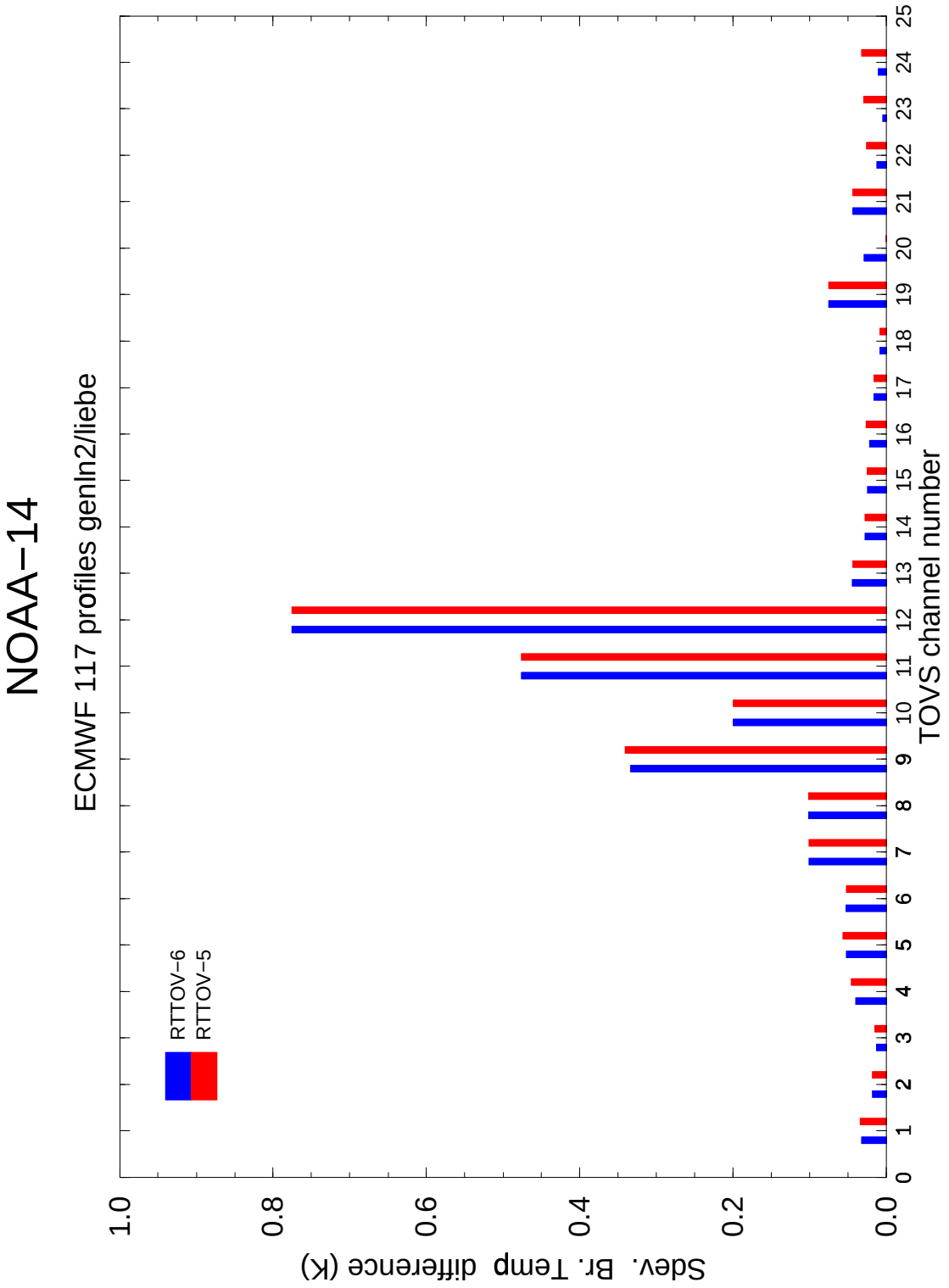

Figure 12 Standard deviations of RTTOV-5 and RTTOV-6 top of atmosphere brightness temperature differences from LbL for the 117 independent profile set for NOAA-14 TOVS. Channels 1-20 are HIRS and 21-24 MSU.

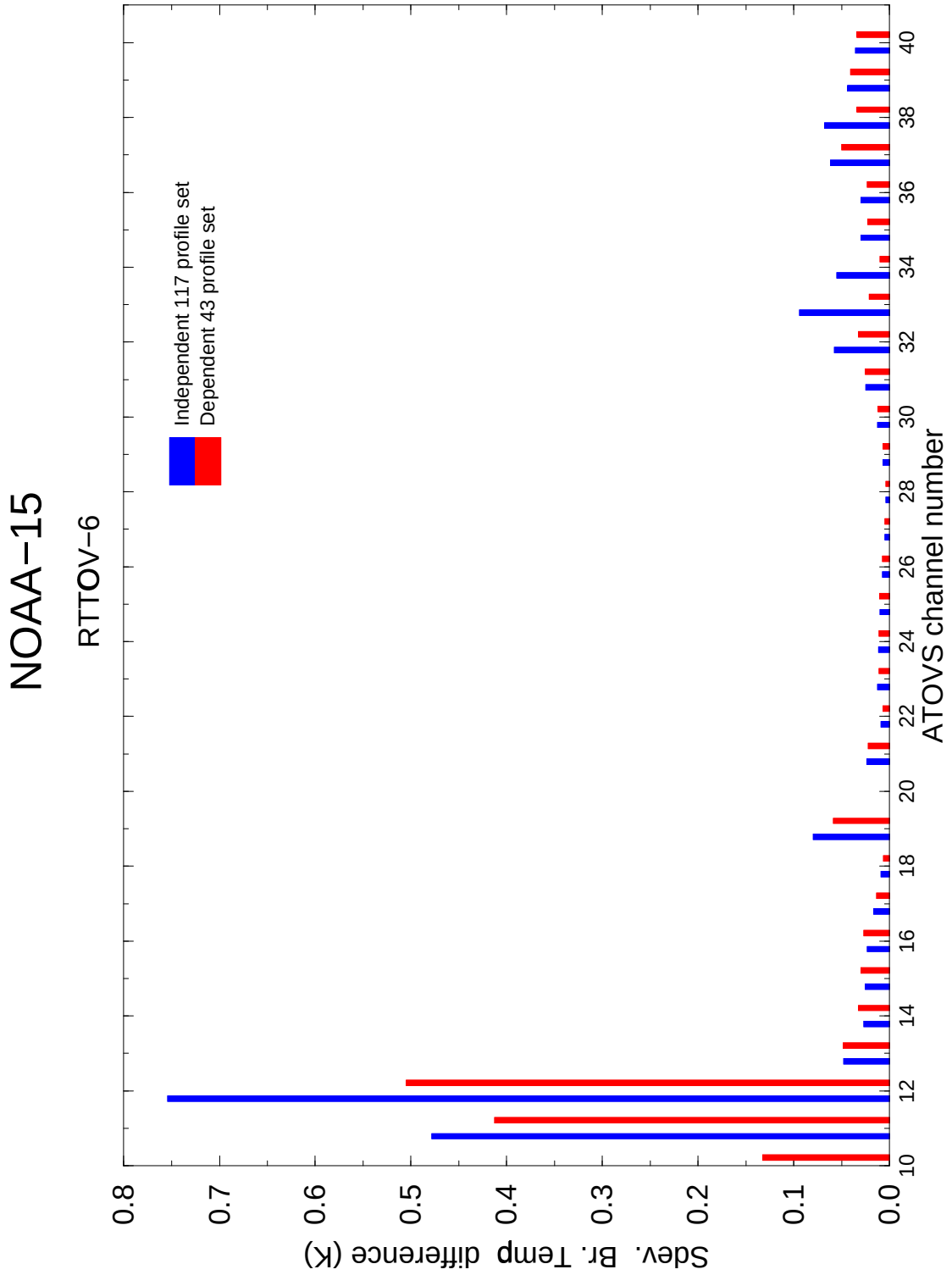

Figure 13 Comparison of standard deviation of brightness temperature differences for dependent and independent profile sets for NOAA-15 ATOVS. (Note that ozone variability is not included in the dependent set so only those channels unaffected by ozone can be compared).

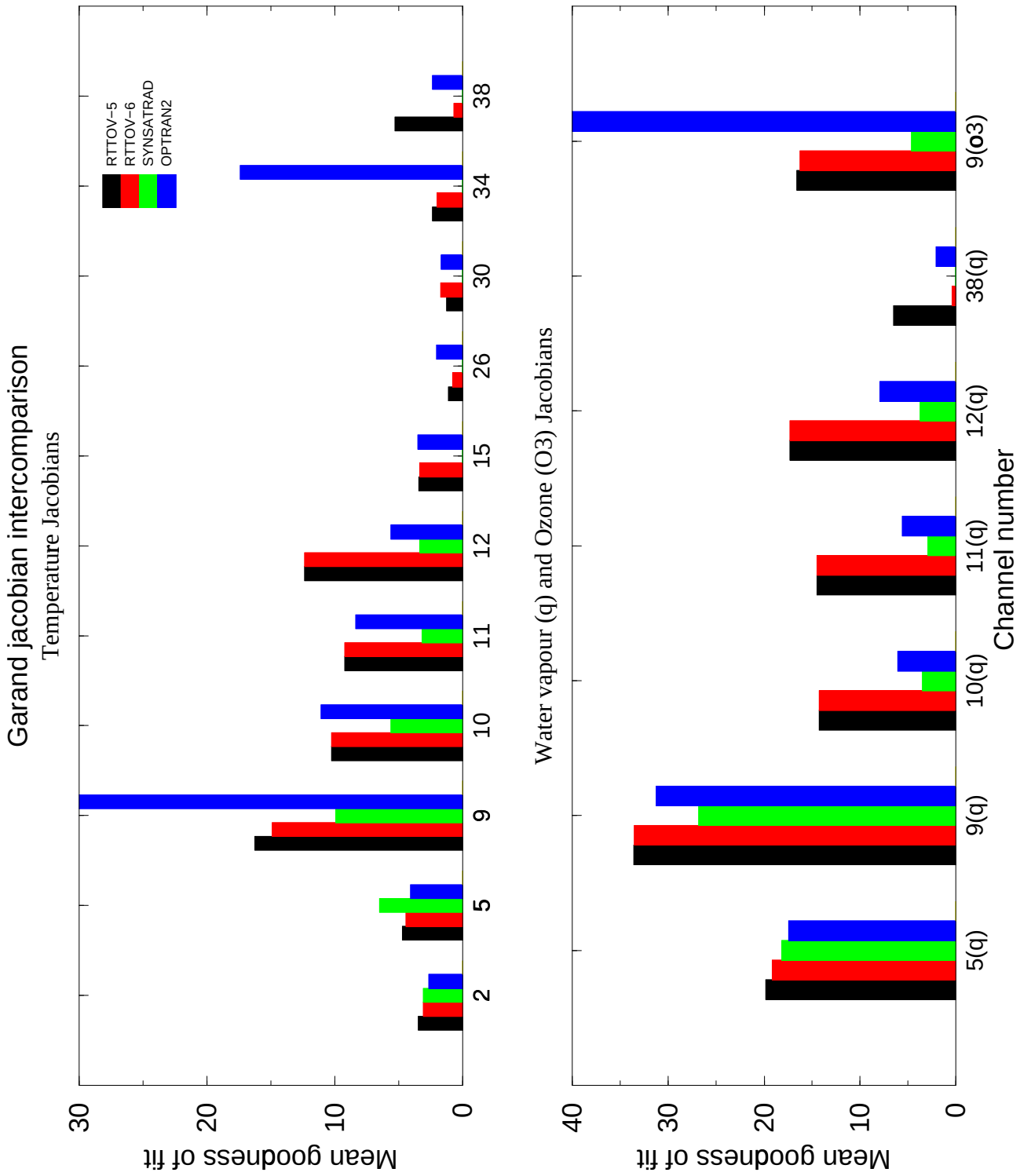

Figure 14 Summary of Garand intercomparison of RT model ATOVS Jacobians for RTTOV-5/6, OPTRAN and SYNSATRAD. Channel numbering is as for Figure 10.

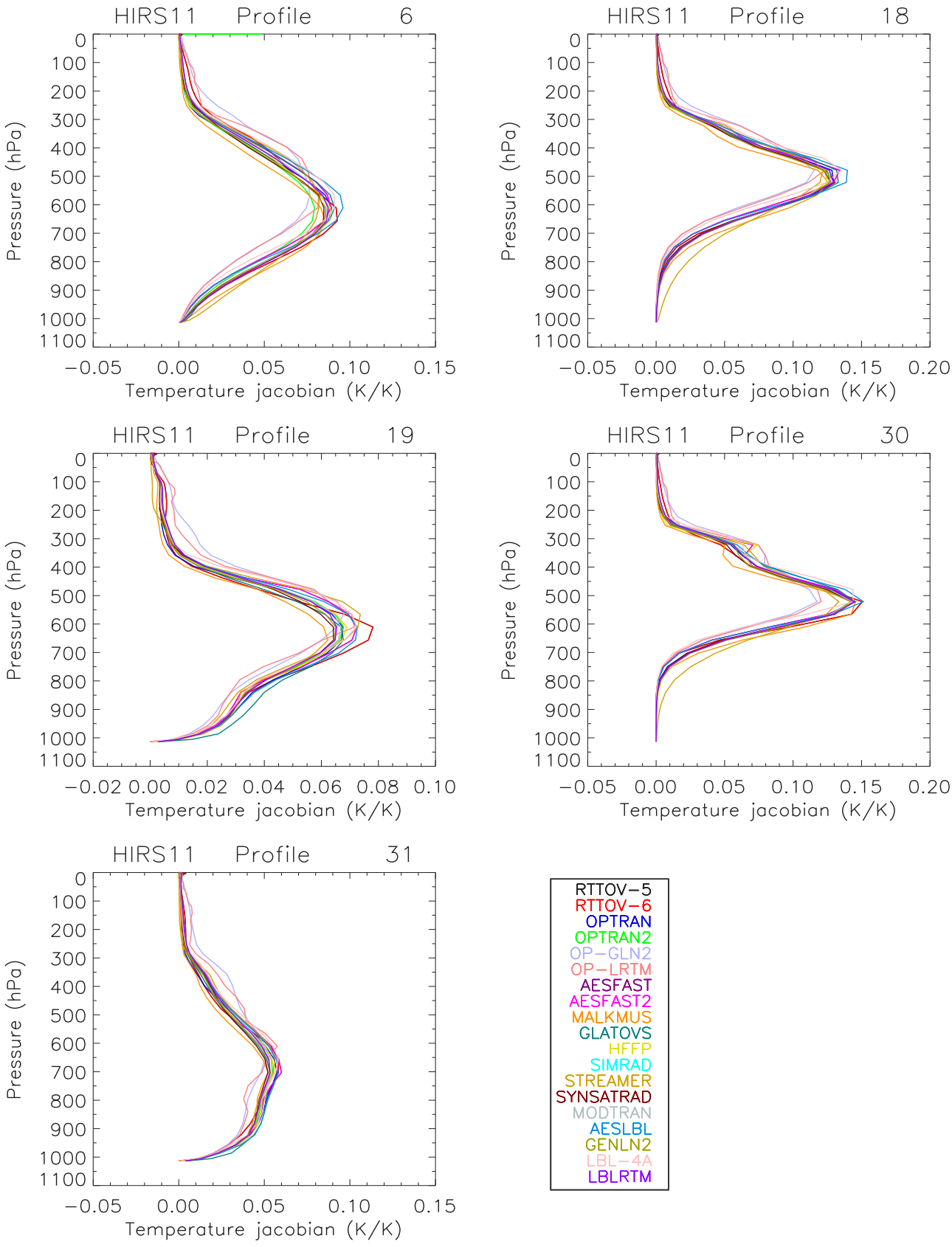

Figure 15 Comparison of temperature jacobians for HIRS channel 11 (from Garand)

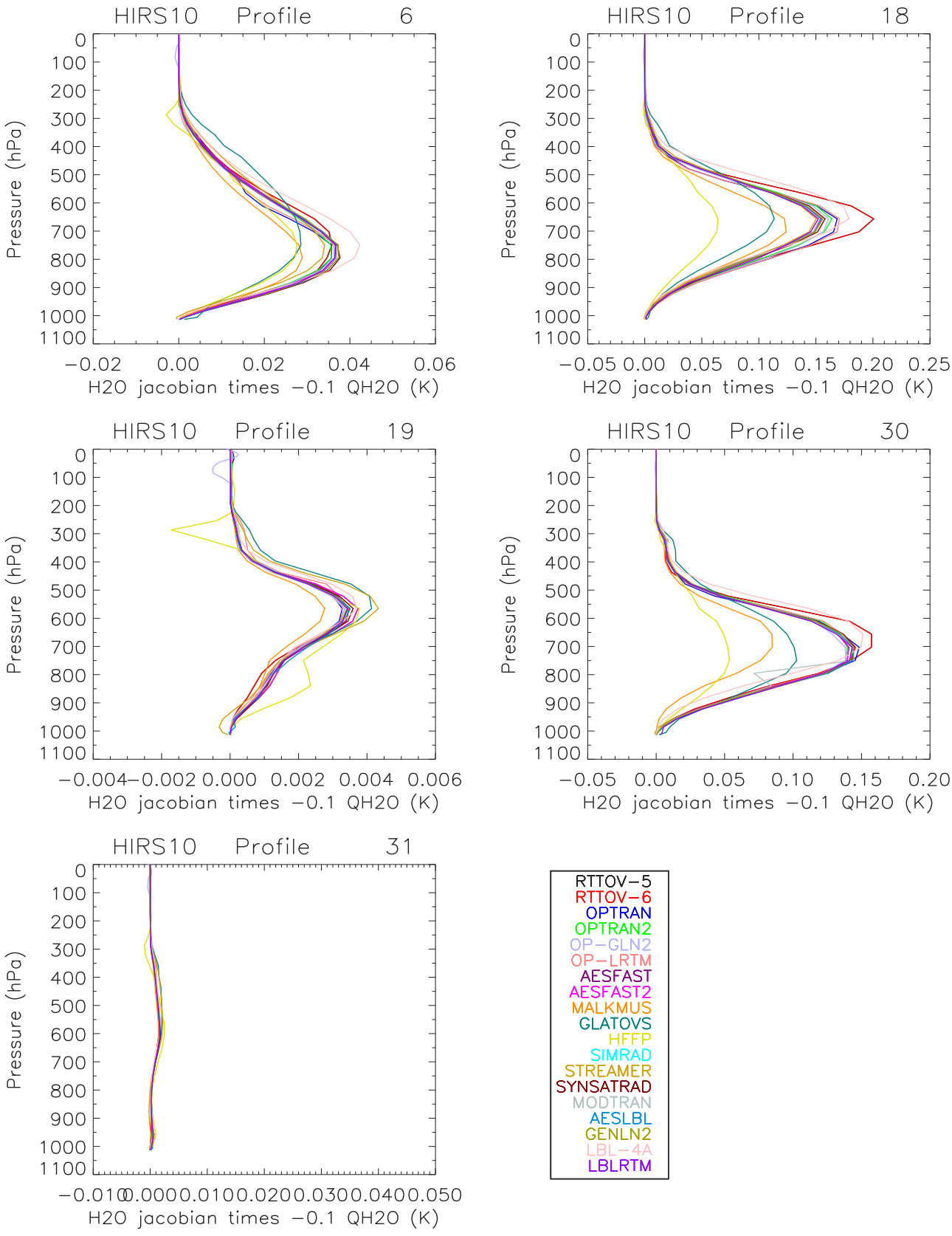

Figure 16 Comparison of water vapour jacobians for HIRS channel 10.

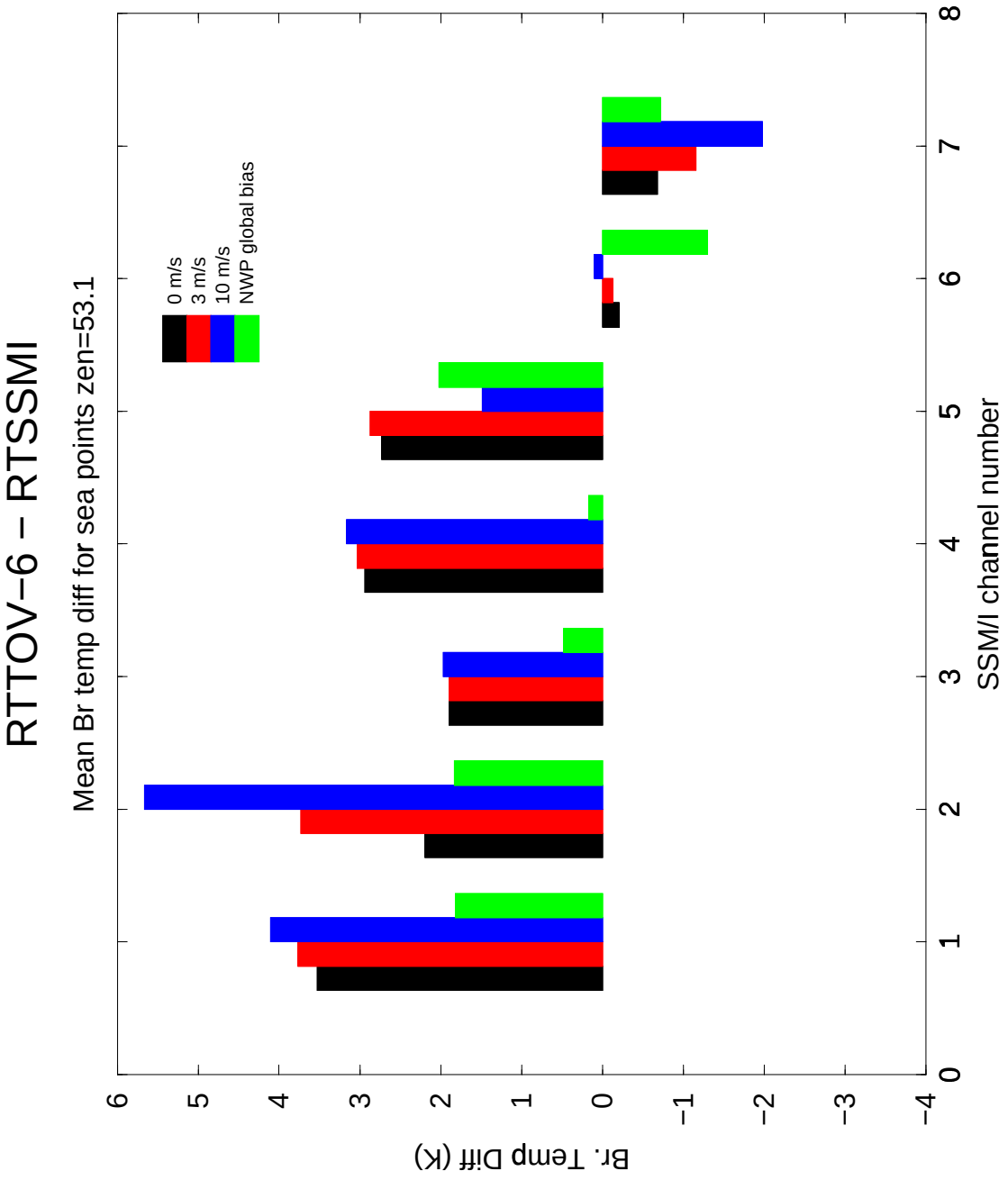

Figure 17 Mean brightness temperature differences for Garand 42 diverse profile set between RTTOV-6 and RTSSMI. Also plotted is the mean observed minus model simulated bias.

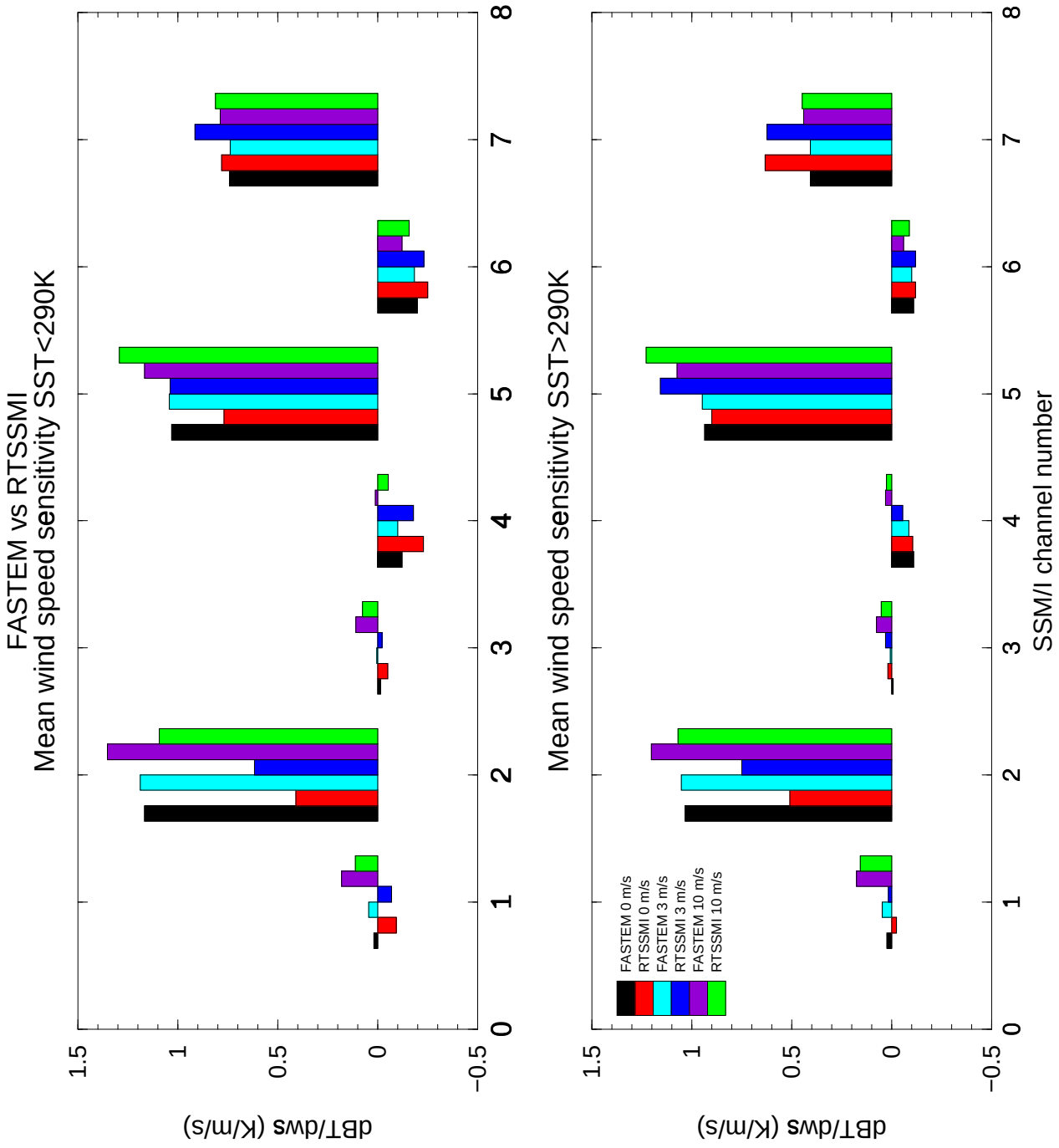

Figure 18 Sensitivity of brightness temperatures to windspeed for FASTEM and RTSSMI for two different SST regimes.

End Of Report